International Journal of Pharmaceutical Science and Research
www.pharmacyjournal.net
ISSN: 2455-4685
Received: 10-08-2025, Accepted: 09-09-2025, Published: 24-09-2025
Volume 10, Issue 2, 2025, Page No. 21-27

Computational design and profiling of novel 1,2-benzisothiazole derivatives as multi-target anticancer agents

Abbas H Abdulsada
Department of Pharmaceutical Chemistry, College of Pharmacy, University of Babylon, Babylon, Iraq

Abstract
Cancer remains a critical global health challenge, necessitating the continuous development of novel and effective therapeutic agents. The 1,2-benzisothiazole scaffold is a privileged structure in medicinal chemistry, renowned for its diverse pharmacological profile. This study employed an integrated computational strategy to design and evaluate ten new 1,2-benzisothiazole derivatives, strategically modified at the R1 and R2 positions, as prospective anticancer agents. *In silico* ADMET profiling using SwissADME predicted all compounds to possess excellent drug-likeness, high gastrointestinal absorption, and favorable pharmacokinetic properties. Induced-fit docking studies against six key oncology targets (COX-1, COX-2, DHFR, MMP13, FGFR1, and NEP) revealed strong binding affinities, with the introduction of a nitro group at R1 consistently enhancing activity. Compounds **7**, **9**, and **10** emerged as top multi-target binders. Molecular dynamics simulations confirmed the stability of these complexes over a 50 ns trajectory, demonstrating low RMSD values and persistent interactions. These results identify the designed 1,2-benzisothiazole derivatives, particularly **9**, as highly promising lead candidates for further experimental development as anticancer therapeutics.

Keywords: 1,2-Benzisothiazole, molecular docking, molecular dynamics, admet, anticancer agents, multi-target agents

Introduction

Cancer remains a paramount challenge to global health, necessitating the continuous discovery of novel therapeutic agents with improved efficacy and reduced off-target effects. In this pursuit, nitrogen- and sulfur-containing heterocyclic scaffolds have emerged as privileged structures in medicinal chemistry due to their structural versatility and widespread presence in pharmacologically active molecules. Among these, the 1,2-benzisothiazole nucleus has attracted significant interest as a versatile pharmacophore, demonstrating a broad spectrum of biological activities. The scaffold's appeal is enhanced by its synthetic accessibility and the potential for extensive structural modification at the N-2 and C-3 positions, allowing for the fine-tuning of physicochemical and pharmacological properties to target specific disease pathways [1, 2].

Extensive research has documented the robust and diverse biological profile of 1,2-benzisothiazole derivatives. Numerous studies have reported potent antimicrobial and antiviral efficacy, as evidenced by novel saccharinyl acetic acid compounds, 3-(alkyl/arylamino) benzo[d]isothiazole derivatives, and inhibitors of the Dengue virus NS2B-NS3 protease [1, 4]. Crucially, and most relevant to the present study, the anticancer potential of this chemotype has been experimentally validated. A novel derivative was demonstrated to inhibit solid tumor growth *in vivo* through potent anti-angiogenesis and apoptosis induction pathways, a finding supported by other computational and *in vitro* studies [5, 6]. The incorporation of this nucleus into pharmacologically active frameworks such as urea, thiourea, hydrazone, oxazolidinone, and piperazine derivatives has further expanded its chemical space, yielding molecules with enhanced cytotoxicity and selectivity [7, 11]. Furthermore, studies on conformational flexibility, probed through advanced techniques like matrix-isolation spectroscopy and quantum chemical calculations, provide a solid foundation for rational drug design [12, 14].

Building upon this established groundwork, the present study employs an integrated computational approach to design and evaluate new 1,2-benzisothiazole derivatives as prospective anticancer agents. A focused library of ten novel compounds was designed by introducing systematic substitutions at the R1 and R2 positions of the core 1,2-benzisothiazole scaffold, exploring a range of electron-donating and electron-withdrawing groups to modulate electronic and steric properties. These compounds will be subjected to *in silico* Absorption, Distribution, Metabolism, and Excretion (ADME) profiling to predict their pharmacokinetic suitability. Furthermore, molecular docking studies will be conducted to elucidate potential binding modes and affinity towards a selected panel of oncology-related protein targets, providing insights into the structure-activity relationship (SAR). To dynamically assess the stability of the ligand-protein complexes and validate the docking predictions, molecular dynamics (MD) simulations will be performed. This comprehensive multi-step computational strategy aims to identify promising 1,2-benzisothiazole-based lead compounds with favorable drug-like properties for subsequent synthetic and biological evaluation.

Computational Method

1. In silico drug-likeness and ADMET prediction

The preliminary assessment of the drug-likeness and pharmacokinetic profile of the ten designed compounds (1-10) (Table 1) was conducted through *in silico* computational methods. The physicochemical properties and key Absorption, Distribution, Metabolism, Excretion, and Toxicity (ADMET) parameters were estimated utilizing the SwissADME online tool (http://www.swissadme.ch/index.php) [15, 17]. This platform provides a comprehensive analysis of properties critical for oral bioavailability, including gastrointestinal (GI)

absorption, blood-brain barrier (BBB) penetration, and P-glycoprotein (Pgp) substrate status.

Table 1: The chemical structure of the proposed compounds

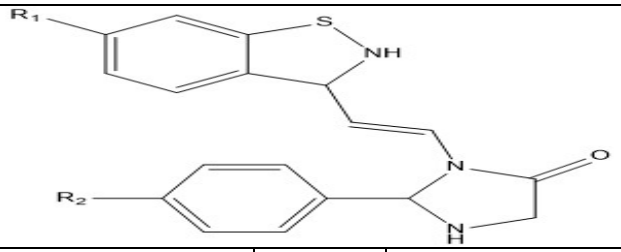

Ligand ID	R1	R2
1	H	H
2	H	OCH_3
3	H	NH_2
4	H	$N(CH_3)_2$
5	H	Cl
6	NO_2	H
7	NO_2	OCH_3
8	NO_2	NH_2
9	NO_2	$N(CH_3)_2$
10	NO_2	Cl

2. Induced-Fit Docking Studies

Molecular docking simulations were performed to evaluate the binding affinity and mode of interaction between the ten designed ligands (**1-10**) and six distinct protein targets: Cyclooxygenase-1 (COX-1, PDB: 3KK6), Cyclooxygenase-2 (COX-2, PDB: 4M11), Dihydrofolate Reductase (DHFR, PDB: 5SDB), Matrix Metalloproteinase-13 (MMP13, PDB: 5UWK), Fibroblast Growth Factor Receptor 1 (FGFR1, PDB: 3TT0), and Neprilysin (NEP, PDB: 6SUK). All simulations were conducted using the Molecular Operating Environment (MOE) software suite, version 2024.06.

Ligand Preparation. The 3D chemical structures of the designed compounds (Table 1) were constructed within MOE. Each structure was energy-minimized using the MMFF94x forcefield. Protonation states were assigned at physiological pH (7.4) using the Protonate3D utility to ensure chemical accuracy prior to docking [18, 19].

Protein Preparation. The crystal structures of the target proteins were obtained from the RCSB Protein Data Bank (PDB). The preparation protocol involved: removal of water molecules and all original co-crystallized ligands, addition of hydrogen atoms, and correction of atom connectivity and bond orders. The resulting structures were subsequently energy-minimized using the AMBER10: EHT forcefield until a root mean square gradient of 0.05 $kcal \cdot mol^{-1} \cdot Å^{-2}$ was achieved, fixing the heavy atoms of the backbone to preserve the native fold [18, 19].

Docking Protocol. Induced-fit docking (IFD) simulations were carried out to account for both ligand and receptor flexibility, which is critical for accurate pose prediction. The docking site was defined by the centroid of the original co-crystallized ligand in each protein structure. The induced-fit methodology was executed in a two-stage process: (i) an initial placement phase using the Triangle Matcher algorithm, generating 30 poses per ligand, and (ii) a refinement phase where the top 10 poses per ligand and their surrounding protein residues (within 6.0 Å) were subjected to sidechain refinement and energy minimization. The binding affinity of each final pose was evaluated using the GBVI/WSA dG scoring function. The stability and reliability of the top-scoring docking pose for each complex were assessed by its Root Mean Square Deviation (RMSD) value relative to the initial placement [20, 21].

3. Molecular dynamics simulations

Molecular dynamics (MD) simulations were performed using the Schrödinger 2021-2 suite to investigate the stability and interaction characteristics of the ligand 7–DHFR complex. The simulation was carried out under an NPT ensemble at 300 K for a total duration of 50 nanoseconds. The system underwent initial minimization and equilibration to ensure the stability of the complex before the production run. Trajectory analysis provided key dynamic descriptors, including Root Mean Square Deviation (RMSD), Root Mean Square Fluctuation (RMSF), and detailed protein-ligand interaction profiles. The protein backbone served as the reference structure for RMSD and RMSF calculations to monitor conformational stability and flexibility. Ligand behavior and fluctuations were evaluated relative to the protein to elucidate binding dynamics within the pocket. Protein-ligand interactions—such as hydrogen bonds, hydrophobic contacts, ionic interactions, and water bridges—were thoroughly characterized to offer comprehensive insights into the molecular recognition mechanism [22, 23].

Results and Discussion

1. Evaluation of Drug-Likeness and ADMET Properties

The computed physicochemical, drug-likeness, and ADMET parameters for the synthesized compounds (1-10) are systematically presented in Table 3. The analysis of these parameters provides crucial insights into their potential pharmacokinetic behavior. A consistent and favorable profile is observed across all ten compounds. Notably, every compound is predicted to exhibit high gastrointestinal (GI) absorption, suggesting a strong potential for effective oral bioavailability. This is a fundamental requirement for the development of orally administered therapeutics.

Regarding distribution properties, the majority of compounds (1-4, 6-10) are predicted not to cross the blood-brain barrier (BBB), which would be a desirable trait for drug candidates targeting peripheral systems, as it minimizes the potential for central nervous system (CNS)-related side effects. A single exception is compound 5, which is predicted to be BBB permeable. This property could be advantageous or disadvantageous depending on the specific therapeutic target (e.g., for a CNS-active drug versus a peripheral agent). All compounds are predicted to be substrates for P-glycoprotein (Pgp), an efflux transporter. This indicates a potential risk for reduced intracellular concentration and possible multidrug resistance, which may need to be addressed in subsequent optimization cycles.

The analysis of fundamental physicochemical properties reveals excellent adherence to Lipinski's Rule of Five, a benchmark for drug-likeness. The molecular weights (MWT) for all compounds range from 323.41 to 396.51 g/mol, well below the 500 Da threshold. The number of hydrogen bond acceptors (nHBA: 3-5) and donors (nHBD: 2-3) are within the recommended limits (≤10 and ≤5, respectively). The topological polar surface area (TPSA) values, ranging from 69.67 to 104.92 $Å^2$, are consistent with good cell permeability for most compounds, though the

higher values (e.g., in 3 and 8) may influence passive diffusion. The calculated partition coefficients (iLOGP and WLOGP) suggest moderate lipophilicity for the series. Furthermore, the consistent synthetic accessibility (SA) score of 0.55 for all compounds indicates they are predicted to be readily synthesizable, facilitating future experimental work.

In conclusion, the *in silico* ADMET profiling indicates that the designed compounds possess strong drug-like characteristics, with high predicted oral absorption and generally favorable physicochemical properties. The uniform Pgp substrate status and the BBB permeability of compound 5 are notable findings that will inform the selection of lead compounds for further *in vitro* and *in vivo* experimental validation.

Table 2: The physicochemical properties, drug-likeness, and drug-likeness scores of the designed compounds

ID	GI	BBB	Pgp	BS	MWT	nHBA	nHBD	TPSA(Å)	iLOGP	WLOGP	nLV
1	High	No	Yes	0.55	323.41	3	2	69.67	2.84	1.19	0
2	High	No	Yes	0.55	353.44	4	2	78.90	2.91	1.20	0
3	High	No	Yes	0.55	338.43	3	3	95.69	2.37	0.78	0
4	High	No	Yes	0.55	366.48	3	2	72.91	3.27	1.26	0
5	High	Yes	Yes	0.55	357.86	3	2	69.67	2.89	1.84	0
6	High	No	Yes	0.55	353.44	4	2	78.90	3.19	1.20	0
7	High	No	Yes	0.55	383.46	5	2	88.13	3.06	1.21	0
8	High	No	Yes	0.55	368.45	4	3	104.92	2.80	0.79	0
9	High	No	Yes	0.55	396.51	4	2	82.14	3.46	1.27	0
10	High	No	Yes	0.55	387.88	4	2	78.90	3.42	1.85	0

2. Induced Fit Docking Studies

The binding energies (scores, kcal/mol) and the associated RMSD values for the top-ranked poses of ligands 1-10 within the active sites of the six target proteins are summarized in Table 2. The results demonstrate a wide range of binding affinities, highlighting the impact of structural modifications on target engagement. A critical analysis reveals that all designed compounds exhibit strong, nanomolar-range predicted binding affinities (score < -7.0 kcal/mol) against most targets, suggesting their potential as multi-target agents. Notably, the introduction of a nitro group (-NO_2) at the R1 position consistently enhanced binding affinity across several targets. This is particularly evident for the COX enzymes. For instance, compound 9 (R1 = NO_2, R2 = $N(CH_3)_2$) emerged as the most potent putative inhibitor for both COX-1 (Score: -9.23 kcal/mol) and COX-2 (Score: -9.42 kcal/mol). Similarly, compounds with the -NO_2 substituent (6-10) generally showed superior scores against MMP13 and FGFR1 compared to their unsubstituted analogs (1-5).

The strong affinity for COX-2 over COX-1 for several ligands (e.g., 7, 9, 10) is a highly desirable characteristic, suggesting a potential for improved selectivity that could mitigate the side effects associated with non-selective COX inhibition. Against DHFR, compounds 7 and 9 again displayed the highest binding affinity (Scores: -8.67 and -8.51 kcal/mol, respectively), reinforcing the positive contribution of the nitro group. For NEP, a different structure-activity relationship was observed, where halogen substitution proved favorable; compounds 5 (R2 = Cl) and 10 (R1 = NO_2, R2 = Cl) were the top-scoring ligands (Scores: -8.64 and -8.50 kcal/mol, respectively). The low RMSD values (generally < 2.0 Å) for the top-scoring poses across all complexes indicate that the final refined docking conformations are structurally consistent with the initial placement, lending credibility to the predicted binding modes and the calculated scores.

In conclusion, the induced-fit docking results successfully predict that the designed ligands can form stable complexes with high affinity for all six targeted enzymes. The systematic variation at the R1 and R2 positions allowed for the identification of key structural features that enhance binding, most notably the nitro group at R1. Compounds 7, 9, and 10 consistently rank among the top binders for multiple targets, making them promising lead candidates worthy of further experimental investigation to validate their predicted multi-target inhibitory activity.

Table 3: The binding scores (kcal/mol) of the designed ligands with potential targets.

proteins		ligands									
		1	2	3	4	5	6	7	8	9	10
3KK6 (COX 1)	score	-7.81	-8.44	-8.24	-8.52	-7.93	-8.66	-8.98	-8.54	-9.23	-8.82
	RMSD	0.90	0.82	1.40	1.50	1.47	1.31	1.36	1.77	1.35	1.16
4M11 (COX 2)	score	-8.29	-8.73	-8.52	-8.33	-8.36	-8.65	-9.05	-8.87	-9.42	-8.81
	RMSD	1.38	1.25	1.63	1.24	0.89	1.30	1.35	1.71	1.51	1.17
5SDB (DHFR)	score	-7.59	-8.03	-7.36	-8.11	-7.53	-8.00	-8.67	-7.73	-8.51	-7.78
	RMSD	1.93	1.86	1.81	1.15	0.85	1.38	1.03	1.30	1.46	1.72
5UWK (MMP13)	score	-7.98	-7.66	-8.00	-8.24	-7.62	-8.75	-8.60	-7.84	-8.48	-7.72
	RMSD	1.70	1.65	1.55	1.93	1.13	1.52	1.90	1.67	1.82	1.78
3TT0 (FGFR1)	score	-7.02	-7.21	-6.88	-7.30	-6.76	-7.24	-7.52	-7.50	-7.41	-7.44
	RMSD	1.65	1.27	1.35	1.56	1.38	1.51	1.79	1.76	1.20	1.72
6SUK (NEP)	score	-7.70	-7.79	-7.67	-7.77	-8.64	-6.64	-7.49	-7.72	-7.64	-8.50
	RMSD	1.27	1.73	1.11	1.41	0.98	0.95	1.53	0.87	1.23	1.97

3. Molecular Dynamics Simulation

1.1 Root Mean Square Deviation (RMSD) Analysis

The structural stability of the protein and the positional fidelity of the ligand within its binding pocket were assessed by calculating the Root Mean Square Deviation (RMSD).

Protein RMSD: The Cα atoms of the protein backbone exhibited an RMSD that stabilized around 1.5 - 2.0 Å after an initial equilibration phase of approximately 5 ns (Figure 2). The fluctuations throughout the remainder of the simulation were confined within this range, indicating that the system had reached equilibrium. The magnitude of the RMSD is within the acceptable threshold of 1-3 Å for a globular protein of this size, suggesting the protein maintained a stable conformational state throughout the 50.2 ns simulation without undergoing large-scale structural rearrangements.

Ligand RMSD: The ligand heavy atom RMSD, calculated after superposition on the protein backbone ('Lig fit Prot'), remained consistently low, fluctuating around 1.0 - 2.0 Å (Figure 2). The close alignment of the ligand RMSD with that of the protein, and its low absolute value, strongly suggests that the ligand remained stably bound within its original binding pocket for the duration of the simulation. There is no evidence of ligand dissociation or significant reorientation within the binding site.

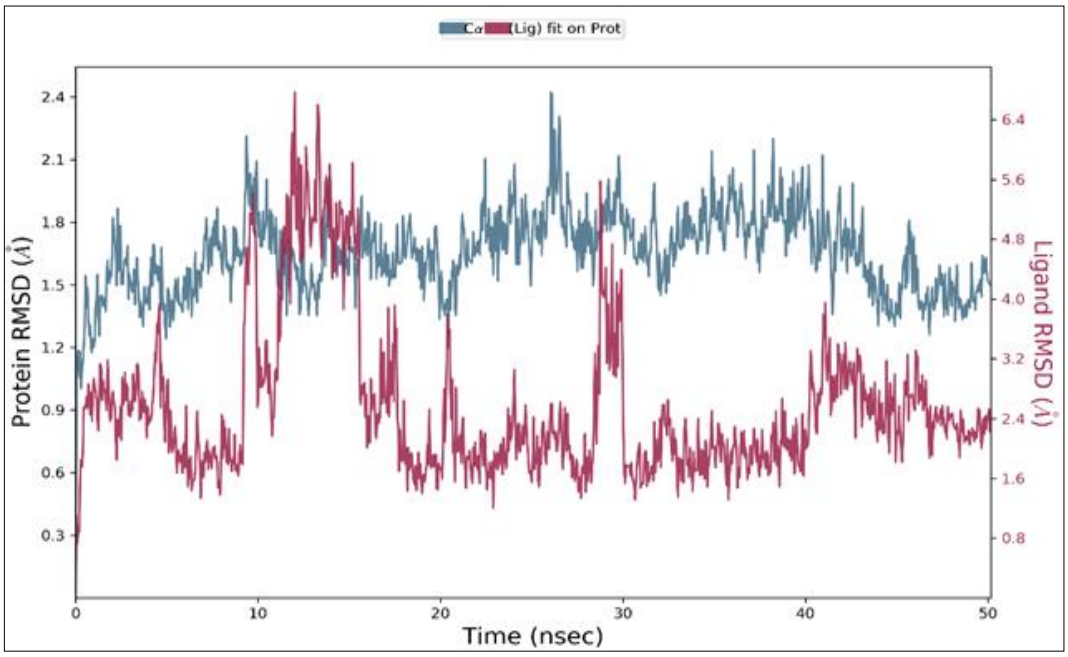

Fig 1: ligand and protein RMSD

1.2 Root Mean Square Fluctuation (RMSF) Analysis

The local flexibility of the protein and ligand was evaluated by computing the Root Mean Square Fluctuation (RMSF).

Protein RMSF: As anticipated, the highest fluctuations were observed in the N- and C-terminal regions, as well as in various loop segments connecting secondary structural elements (Figure 3). The core secondary structures, such as alpha-helices and beta-strands, demonstrated lower RMSF values, confirming their structural rigidity. Several residues identified as making contact with the ligand (marked with green vertical bars) displayed low to moderate fluctuations, which is consistent with their role in forming a stable binding pocket.

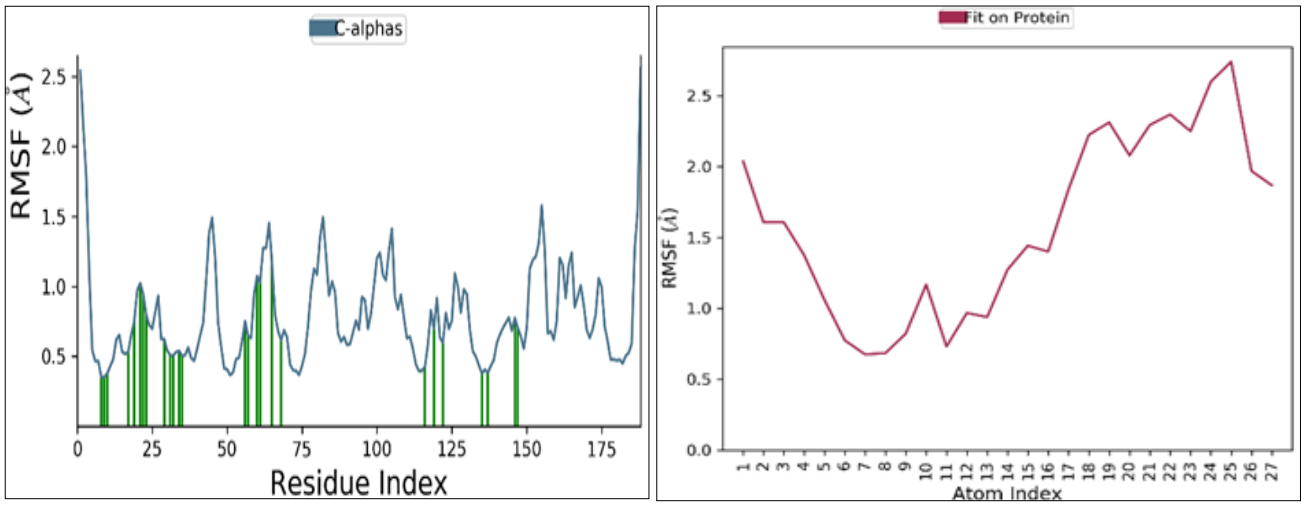

Fig 2: A. protein RMSF and B. ligand RMSF

Ligand RMSF: The RMSF of individual ligand atoms provides insight into the flexibility of specific functional groups (Figure 5). The analysis indicates that while the core scaffold of the ligand is rigid, certain terminal and linker regions (e.g., around torsion 5) exhibit higher flexibility. This mobility is likely important for achieving optimal interactions with the protein and accommodating minor conformational changes during binding.

1.3 Ligand-Protein Contacts

The ligand-protein contacts analysis reveals specific atomic-level interactions between the ligand and protein residues that persist for more than 30% of the simulation time. Key residues such as THR_57, VAL_116, PHE_35, and ILE_17 demonstrate stable interactions, predominantly hydrophobic and polar in nature, with occasional water-mediated bridges. The persistence of these interactions suggests a well-defined binding mode, with hydrophobic residues forming a stable core around the ligand, while polar and water-bridged contacts contribute to the specificity and solvation of the binding site. The presence of multiple interaction types with high occupancy indicates a favorable binding affinity and structural complementarity between the ligand and the protein's active site.

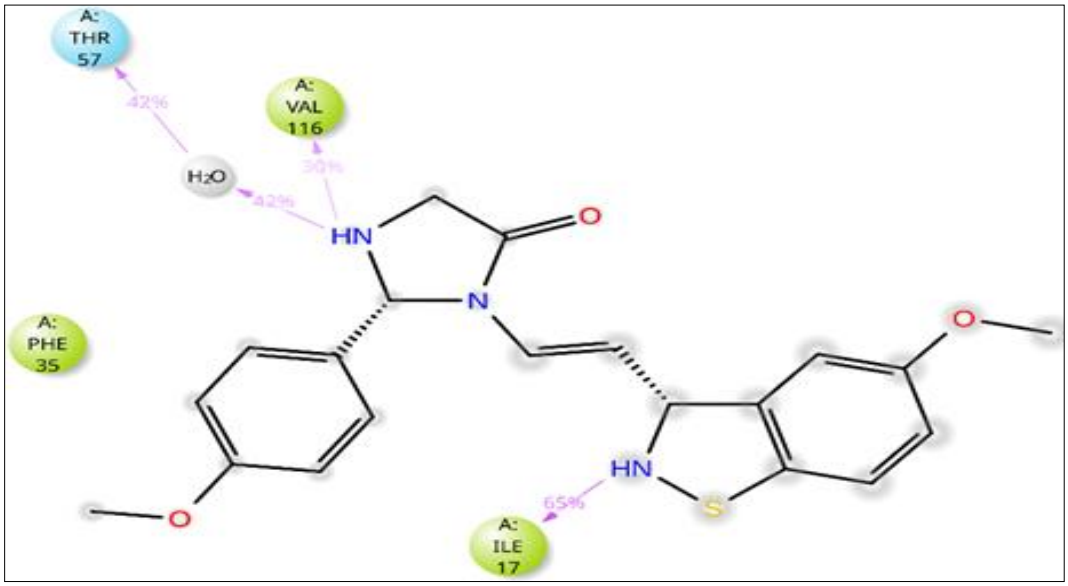

Fig 3: Ligand-Protein Contacts

1.4 Protein-Ligand Contacts

The protein-ligand contacts overview illustrates the temporal evolution and diversity of non-covalent interactions throughout the simulation. Hydrogen bonds, hydrophobic contacts, ionic interactions, and water bridges are quantified, with hydrophobic interactions being the most prevalent, followed by hydrogen bonds involving residues such as ASP_22, TYR_34, and SER_60. The stability of these interactions over 50 ns, as shown in the timeline and normalized occupancy plots, indicates that the ligand remains tightly bound within the pocket without significant dissociation. The consistent involvement of specific residues across multiple interaction types underscores the robustness of the binding pose and supports the potential of the ligand as a strong binder with minimal positional fluctuation.

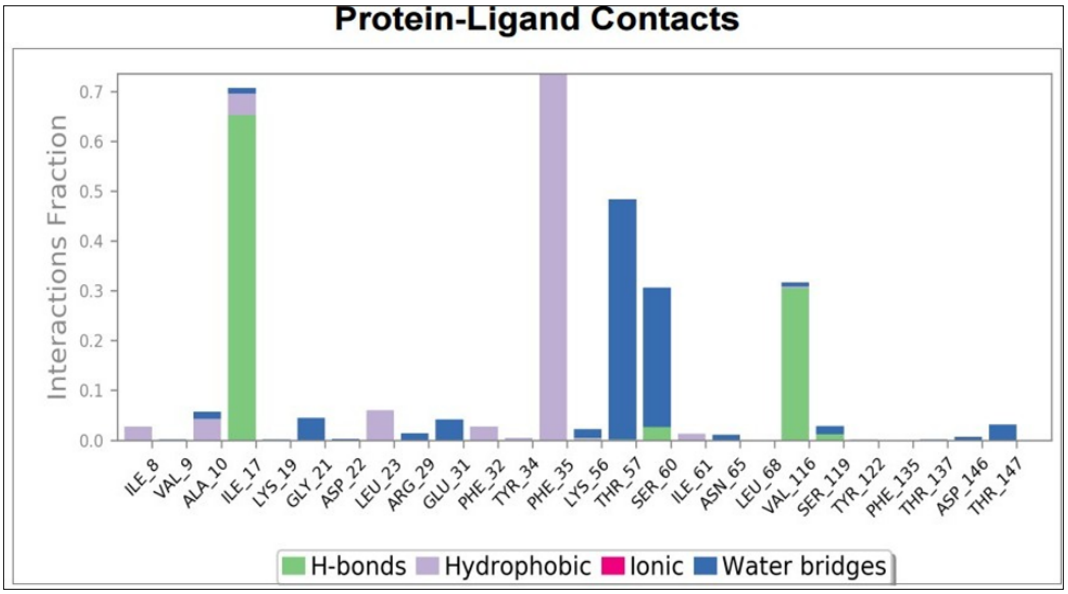

Fig 4: Protein-Ligand Contacts

Conclusion

This comprehensive *in silico* investigation successfully demonstrates the significant potential of a novel series of 1,2-benzisothiazole derivatives as multi-target anticancer agents. The systematic substitution at the R1 and R2 positions allowed for the exploration of structure-activity relationships, revealing that electron-withdrawing groups, particularly a nitro group at R1, markedly enhanced binding affinity across a panel of protein targets. The ADMET predictions confirmed the drug-like character and promising pharmacokinetic profiles of all designed compounds. Molecular docking and subsequent molecular dynamics simulations provided atomic-level validation, confirming stable binding modes and high-affinity interactions for the top-ranking compounds, notably 7, 9, and 10. The convergence of favorable predicted ADMET properties, potent multi-target binding affinity, and complex stability strongly advocates for these hits, especially compound 9 (R1 = NO_2, R2 = $N(CH_3)_2$), to be advanced to synthetic and biological evaluation. This study provides a robust rational foundation for the development of a new class of 1,2-benzisothiazole-based anticancer drugs.

Declaration of Competing Interest

There are no conflicts to declare

Acknowledgement

The authors would like to thank University of Babylon (https://www.uobabylon.edu.iq/) in Babylon, Iraq, for their support in completing this work.

References

1. Abdellattif M. Synthesis of Some Novel Compounds of Saccharinyl Acetic Acid Containing Nucleus and Evaluation of Their Biological Activities as Antimicrobial. Oriental Journal of Chemistry,2016:32(1):565–574.
2. Kamble DP, Shankarwar AG, Mane Y, Tigote R, Sarnikar YP, Madje BR. Synthesis, Characterization and Antimicrobial Evaluation of New 3-(Alkyl/Arylamino) benzo [d] isothiazole 1,1-Derivatives. Oriental Journal Of Chemistry,2021:37(4):797–804.
3. Batool F, Saeed M, Saleem HN, Kirschner L, Bodem J. Facile Synthesis and *In vitro* Activity of N-Substituted 1,2-Benzisothiazol-3(2H)-ones against Dengue Virus NS2BNS3 Protease. Pathogens,2021:10(4):464.
4. Lin ZS. Benzisothiazole based anti-viral agents: new chemistry revealed during structure-activity relationship studies [PhD dissertation]. Vancouver (BC): University of British Columbia, 2020 Aug.
5. Kungyal T, Salimath BP. A novel derivative of benzisothiazole inhibits solid tumor growth *in vivo* by anti-angiogenesis and apoptosis. Res J Life Sci Bioinform Pharm Chem Sci,2019:5(5):71–81.
6. Kungyal T, Mutahar AZ, Salimath BP. Computational, *in vitro* and *in vivo* studies to evaluate anti-cancer activity of benzisothiazole derivative. Deleted Journal,2019:8(7):272–278.
7. Sharma A, Suhas R, Chandana KV, Banu SH, Gowda DC. tert-Butyl 1,5-bis(4-(benzo[d]isothiazol-3-yl) piperazin-1-yl)-1,5-dioxopentan-2-ylcarbamate urea/thiourea derivatives as potent H+/K+-ATPase inhibitors. Bioorganic & Medicinal Chemistry Letters,2013:23(14):4096–4098.
8. Sharma A, Suhas R, Chandan S, Gowda DC. Novel urea and thiourea derivatives of thiazole-glutamic acid conjugate as potential inhibitors of microbes and fungi. Russian Journal of Bioorganic Chemistry,2013:39(6):656–664.
9. Patekar MR, Medhane VJ, Jadhav GJ, Thakare MJ, Deshmukh DG. Synthesis of (s)-1-{3-[4-(4-benzo[d]isothiazol-3-yl-piperazin-1-yl) -3-fluoro-phenyl] -2-oxo-oxazolidin-5-ylmetyl} -3-substituted-urea derivatives as antibacterial agents. Journal of Heterocyclic Chemistry,2021:58(11):2152–2162.
10. Wang X, Dong M, Meng Z, Chen J, Yang J, Wang X. Synthesis and Biological Activity of Acrylate Copolymers Containing 3-Oxo-N-allyl-1,2-benzisothiazole-3(2H) -carboxamide Monomer as a Marine Antifouling Coating. ChemistryOpen,2021:10(5):523–533.
11. Rollas S, Küçükgüzel S. Biological Activities of Hydrazone Derivatives. Molecules,2007:12(8):1910–1939.
12. Gómez-Zavaglia A, Kaczor A, Coelho D, Cristiano S, Fausto R. Conformational and structural analysis of 2-allyl-1,2-benzisothiazol-3(2H)-one 1,1-dioxide as probed by matrix-isolation spectroscopy and quantum chemical calculations. Journal of Molecular Structure,2008:919(1-3):271–276.
13. Kaczor A, Almeida R, Gómez-Zavaglia A, Fausto R. Molecular structure and infrared spectra of the monomeric 3-(methoxy)-1,2-benzisothiazole 1,1-dioxide (methyl pseudosaccharyl ether). Journal of Molecular Structure,2007:876(1-3):77–85.
14. Almeida R, Gómez-Zavaglia A, Kaczor A, Cristiano MLS, Eusébio MES, Tomé MMR, *et al*. First observation of Chapman rearrangement of a pseudosaccharyl ether in the solid state: the thermal isomerization of 3-(methoxy)-1,2-benzisothiazole 1,1-dioxide revisited. Tetrahedron,2008:64(15):3296–3305.
15. Naglah AM, Askar AA, Hassan AS, Khatab TK, Al-Omar MA, Bhat MA. Biological evaluation and molecular docking with in silico physicochemical, pharmacokinetic and toxicity prediction of pyrazolo [1, 5-a] pyrimidines. Molecules,2020:25(6):1431.
16. Shaikh TT, Adnaik RS, Patil NB. Swiss ADME Predictions of Pharmacokinetics and Drug-Likeness Properties of Chemical Constituents Present in *Embelia ribes*. International Journal of Pharmacy and Pharmaceutical Research,2025:31(1):68–76.
17. Nizamuddin ND, Roopa D, Alla P, Shaik AS, Kumar V, Kapu SR. In – Silico Biological Evaluation of Anticancer Drugs - SWISS ADME. Future Journal of Pharmaceuticals and Health Sciences,2024:4(2):39–55.
18. Abdulsada AH, Al-yassery HK, Abdul Hussein SA. Design, ADME, Molecular Docking, And Molecular Dynamics Simulation Study of Tyrosine Derivatives of Isatin – Isatin-Para-Aminobenzoic Acid Conjugates. Res J Pharm Biol Chem Sci,2025:16(3):69–77.
19. Quazi S, Gavas S, Malik JA, KS S, Haider Z. In-silico pharmacophore and Molecular Docking based drug discovery against Marburg Virus's Viral Protein 35; A potent of MAVD. bioRxiv (Cold Spring Harbor Laboratory), 2021 Jul 3.

20. Nassar H, Sarnow A, Celik I, Abdelsalam M, Robaa D, Sippl W. Ternary Complex Modeling, Induced Fit Docking and Molecular Dynamics Simulations as a Successful Approach for the Design of VHL-Mediated PROTACs Targeting the Kinase FLT3. Archiv der Pharmazie,2025:358(4).
21. Szwabowski GL, Castleman PN, Sears CK, Wink LH, Cole JA, Baker DL, *et al*. Benchmarking GPCR homology model template selection in combination with de novo loop generation. Journal of Computer-Aided Molecular Design,2020:34(10):1027–1044.
22. Gheidari D, Mehrdad M, Bayat M. Synthesis, docking, MD simulation, ADMET, drug likeness, and DFT studies of novel furo[2,3-b] indol-3a-ol as promising Cyclin-dependent kinase 2 inhibitors. Scientific Reports,2024:14(1).
23. Priya K, Manandhar S, Sankhe R, Setty MM, Babu U, Pai SR. Structure based virtual docking and molecular dynamics guided identification of potential phytoconstituents from traditionally used female antifertility plant. Pharmaceutical Sciences.